

Detecting superconductivity out-of-equilibrium

S. Paegel,^{1,2} B. Fauseweh,^{3,4} A. Osterkorn,² T. Köhler,^{5,2} D. Manske,³ and S.R. Manmana²

¹*Fakultät für Physik, Ludwig-Maximilians-Universität München, D-80333 München, Germany*

²*Institut für Theoretische Physik, Georg-August-Universität Göttingen, D-37077 Göttingen, Germany*

³*Max-Planck-Institut für Festkörperforschung, Heisenbergstraße 1, D-70569 Stuttgart, Germany*

⁴*Theoretical Division, Los Alamos National Laboratory, Los Alamos, New Mexico 87545, USA*

⁵*Department of Physics and Astronomy, Uppsala University, Box 516, S-751 20 Uppsala, Sweden*

(Dated: February 27, 2020)

Recent pump-probe experiments on underdoped cuprates and similar systems suggest the existence of a transient superconducting state above T_c . This poses the question how to reliably identify the emergence of long-range order, in particular superconductivity, out-of-equilibrium. We investigate this point by studying a quantum quench in an extended Hubbard model and by computing various observables, which are used to identify (quasi-)long-range order in equilibrium. Our findings imply that, in contrast to current experimental studies, it does not suffice to study the time evolution of the optical conductivity to identify superconductivity. In turn, we suggest to utilize time-resolved ARPES experiments to probe for the formation of a condensate in the two-particle channel.

Introduction Superconductivity (SC) is one of the hallmarks of condensed-matter systems and has inspired researchers since its discovery in 1911, and later by the advent of high-temperature SC in cuprate materials [1–4]. While, in particular for the latter class of materials, a lot of questions are subject of ongoing research, many characteristics of the SC phase are by now well established as long as the system is in equilibrium. However, recent experiments (e.g., [5–9] on copper oxides, or on K_3C_{60}) report the observation of possible photo-induced transient SC phases, which can exist at elevated temperatures, even above the equilibrium-critical temperature T_c [10–13]. In these investigations, ultrashort THz pulses excite single phonon modes, which decay very slowly compared to the typical time scale of the electron dynamics and thereby offer the possibility to control the interaction parameters of the electronic system [14]. Subsequently, the ω -dependent optical conductivity is determined as a function of time via reflectivity measurements using a probe pulse, and SC correlations are identified by the emergence or enhancement of a signal at $\omega \rightarrow 0$. This is by now a standard experimental procedure, which, however, leaves many questions open, in particular concerning the characterization of the state induced by the pump excitation (see, e.g., Refs. 15–20).

In this Letter, we address this issue regarding further experimental measures to probe SC in such non-equilibrium setups. For the sake of simplicity, we focus on one-dimensional (1D) systems, for which powerful numerical techniques are available in terms of matrix-product states (MPS) [21–23]. We argue that it does not suffice to study only the optical conductivity, since the pump as well as the probe pulse can induce currents, which can modify the low-frequency behavior, without being a direct proof for SC. Nevertheless, we are able to provide evidence for the emergence of SC in the course of time by studying the time evolution of spectral functions, which are accessi-

ble to variants of time- and angle-resolved photoemission spectroscopy (tr-ARPES) experiments [24–30]. We propose to study the usual single-particle and a pairing spectral function, which we introduce below. We find particularly in the latter quantity clear signatures for the accumulation of weight at $k = 0$. This raises the question, whether a condensation or quasicondensation of pairs is achieved, which would realize a transient non-equilibrium SC state. It is interesting to ask, whether non-equilibrium situations can be beyond the realm of validity of the Mermin-Wagner-Hohenberg theorem [31–33], which inhibits the formation of true long-range order (LRO) in 1D systems. The scope of this Letter is, therefore, three-fold: To demonstrate that the time evolution of the optical conductivity does not suffice to unambiguously establish transient SC order, to present spectral functions as a more reliable probe, and to further characterize the observed transient state by investigating correlation matrices. The general validity of our findings is supported by comparing the extended Hubbard model [34–40] and a variant of the 1D t - J model [3, 41–46].

Model and Methods We study the time evolution of Hubbard chains [47–50] following a quantum quench [51]. Recent experiments [7–9, 11] on high- T_c superconductors suggest that if there exists preformed pairing, e.g., in the normal state slightly above T_c , pumping particular phonon modes induces charge coherences, which drive the system into a transient superconducting state. Therefore, our starting point is to assume that lattice distortions modify the strength of the couplings [10, 14] and thereby alter the nearest-neighbor interaction between the electrons. Thus, we consider a quench in the 1D extended Hubbard model,

$$\hat{H} = \hat{T} + U \sum_j \hat{n}_{j,\uparrow} \hat{n}_{j,\downarrow} + V \sum_j \hat{n}_j \hat{n}_{j+1} \quad (1)$$

with $\hat{T} = -t_{\text{hop}} \sum_{j,\sigma} (\hat{c}_{j,\sigma}^\dagger \hat{c}_{j+1,\sigma} + \text{h.c.})$ being the kinetic energy. Therein, $\hat{c}_{j,\sigma}^{(\dagger)}$ are $S - 1/2$ fermionic ladder operators, which obey the canonical anticommutation relations $\{\hat{c}_{i,\sigma}, \hat{c}_{j,\sigma'}^\dagger\} = \delta_{i,j} \delta_{\sigma,\sigma'}$, $\{\hat{c}_{i,\sigma}, \hat{c}_{j,\sigma'}\} = \{\hat{c}_{i,\sigma}, \hat{c}_{j,\sigma'}^\dagger\} = 0$, and we denote by $\hat{n}_j = \hat{n}_{j,\uparrow} + \hat{n}_{j,\downarrow}$ the total electron occupation at site j . For later convenience, we also define doublon ladder operators $\hat{d}_j \equiv \hat{c}_{j,\uparrow} \hat{c}_{j,\downarrow}$. As motivated above, we start in a charge-density wave (CDW), which favors double occupancies ($U/t_{\text{hop}} = -4$, $V/t_{\text{hop}} = 1/4$) [18, 52]. We perform a sudden quench in the nearest-neighbor interaction $V/t_{\text{hop}} = 1/4 \rightarrow -1/4$ into the s-wave superconducting phase at zero temperature [53], keeping the local Hubbard interaction fixed at $U/t_{\text{hop}} = -4$. Note that this value of the attractive interaction is comparable to the electronic bandwidth. Although this is out of the scope for cuprate high- T_c superconductors, it is, however, similar to the electronic structure in alkali-doped fullerenes, where the effective phonon-mediated intraorbital interaction is comparable to the electronic bandwidth coming from t_{1u} bands [54].

We then calculate the real-time evolution using a combined single- and two-site time-dependent variational principle (TDVP) scheme in the MPS formulation of the density-matrix renormalization group (DMRG) for lattices [21–23, 55] with up to $L = 80$ sites, open boundary conditions, and a maximal bond dimension of $m_{\text{max}} = 1000$ states. By comparing calculations with different values of m_{max} we estimate the accuracy of the presented results to be of a few percent [53]. To investigate the formation and stability of transient SC, we studied the differential optical conductivity after a probe pulse [56, 57], spectral functions, and the correlation matrices [58, 59] of single- and two-particle excitations [24–29, 60–62]. We complement our studies by considering a similar quench in the 1D t - J_\perp model [45, 46], $\hat{H}_{t-J_\perp} = \hat{T} + J_\perp/2 \sum_j (\hat{S}_j^+ \hat{S}_{j+1}^- + \hat{S}_j^- \hat{S}_{j+1}^+)$, at filling $n = 0.2$ by quenching $J_\perp/t_{\text{hop}} = 2 \rightarrow 6$, i.e., from a Luttinger liquid [63] to a singlet SC phase [64]. We choose our energy and time units by setting $t_{\text{hop}} \equiv 1$ and $\hbar \equiv 1$.

Time-dependent Optical Conductivity The experimental setups [7–9, 11] we refer to typically measure the reflectivity after pump-probe excitations, from which the optical conductivity is extracted. We follow Refs. 56 and 57 and compute the differential optical conductivity

$$\sigma(\omega, \Delta t) = \frac{j(\omega, \Delta t)}{i(\omega + i\eta)A(\omega, \Delta t)L} \equiv \sigma_1(\omega, \Delta t) + i\sigma_2(\omega, \Delta t) \quad (2)$$

after the quench at $t = 0$. $A(\omega, \Delta t)$ is the vector potential of the Fourier-transformed Gaussian probe pulse [65] $A(t, \Delta t) = A_0 e^{-\frac{(t-\Delta t)^2}{2\tau^2}} \cos(\omega_0 t)$ in Peierls substitution [66] applied after the time delay Δt . The overall response current

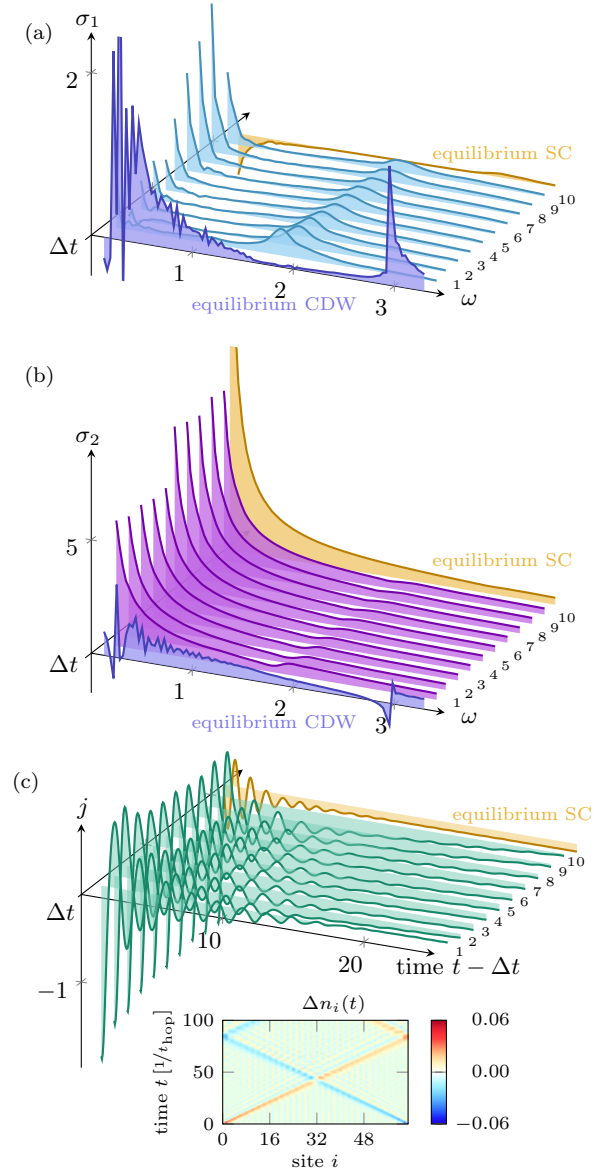


FIG. 1. Real (a) and imaginary (b) part of the optical conductivity $\sigma_{1,2}(\omega, \Delta t)$ with probe pulses applied at different time delays Δt and the corresponding quantities in the CDW ground state (violet) and the SC ground state (orange). The Bottom panel (c) shows the real-time evolution of the response current $j(t - \Delta t, \Delta t)$ after application of a probe pulse at time delay Δt following the quench (green) and in the SC ground state (orange). The charge flow after applying the probe pulse in the SC ground state at $\Delta t = 0$ is shown in the inset.

$j(t, \Delta t) = i \left\langle \sum_{j,\sigma} \left(e^{-iA(t,\Delta t)} \hat{c}_{j,\sigma}^\dagger \hat{c}_{j+1,\sigma} - \text{h.c.} \right) \right\rangle$ was calculated from a real-time evolution of the perturbed system, and the ω -dependence $j(\omega, \Delta t)$ is obtained by a Fourier transform [67] including values up to time $t = 25/t_{\text{hop}}$ after the probe pulse. We show the real (Fig. 1a) and imaginary (Fig. 1b) parts of $\sigma(\omega, \Delta t)$ for delays up to $\Delta t = 10$ and a system with $L = 64$

sites. For the real part, we find a sudden transfer of spectral weight from the CDW signal at around $\omega \approx 3$ towards $\omega \approx 1.7$, which is due to the sudden change of the Hamiltonian. At the same time, in the imaginary part a peak forms near $\omega = 0$. We compare this to the SC ground state and realize that, at the first glance, similar behavior is induced. However, in particular in σ_1 , clear differences appear, and σ_2 shows additional features. Also, it is hard to decide whether $\sigma_2(\omega, \Delta t)$ is diverging as $1/\omega$ for $\omega \rightarrow 0$, since we are limited in the frequency resolution. We conclude that, as in the experiments, the question whether the accumulation of spectral weight near $\omega = 0$ is due to induced SC or an enhanced metallicity after a pump pulse is hard to decide [53]. However, in contrast to the experimental situation we have direct access to the time dependence of the current induced by the probe pulse. The properties of this current are further illustrated by the inset of Fig. 1c, where we display the response electron density $\Delta n_i(t) = \langle \hat{n}_i(t) \rangle_{\text{probe}} - \langle \hat{n}_i \rangle_0$, which compares the time evolution of the local density in the SC phase with and without probe pulse. As can be seen, the effect of the probe pulse is to accumulate charge at the edges of the system. After passage of the probe pulse, this causes the measured current. In the SC phase the probe pulse induces a long-living current, while in non-equilibrium we find no clear evidence for a comparable response (see Fig. 1c). In turn, in our simulations the induced charge flow decays on time scales of at least $t \sim 25/t_{\text{hop}}$ which sets the scale of a low-frequency response $2\pi/t \approx 0.25$ in the imaginary part σ_2 . Thus, a strengthening of the response at $\omega \rightarrow 0$ alone, as observed here, does not suffice to demonstrate SC. This is supported by studying a quench within the CDW phase, in which a similar behavior of the optical conductivity is observed, but without further indication for SC in other observables [53].

Spectral Functions From now on we consider postquench states at $\Delta t = 15/t_{\text{hop}}$. This is justified, since for times $t > 4/t_{\text{hop}}$ a transient state is reached, as seen in the time evolution of the eigenvalues of the correlation matrix, which we find to be non-thermal [53]. Motivated by tr-ARPES, we consider the in- and out-of-equilibrium time-dependent lesser Greens functions for $t > \Delta t$: $C_{\hat{O}}(j, t, \Delta t) = \langle \psi(\Delta t) | \hat{O}_j^\dagger(t) \hat{O}_{L/2}(0) | \psi(\Delta t) \rangle$ in the single- and two-particle channel, i.e., $\hat{O}_j = \hat{c}_{j,\uparrow}$ and $\hat{O}_j = \hat{d}_j$, respectively, and we indicate the equilibrium case by setting $\Delta t \equiv 0$. We refer to the Fourier transform to momentum and frequency space [53]

$$S_{\hat{O}}(q, \omega, \Delta t) = \int_{-\infty}^{\infty} \frac{dt}{2\pi} \sum_j e^{-i(qr_j - (\omega + i\eta)t)} C_{\hat{O}}(j, t, \Delta t), \quad (3)$$

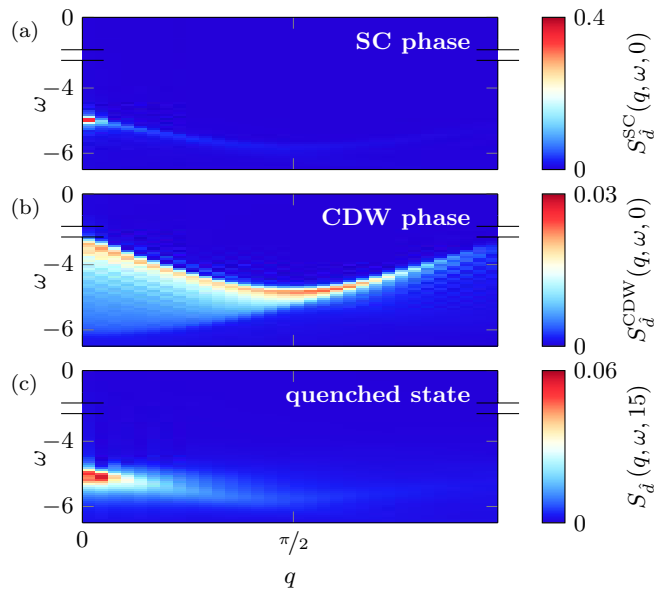


FIG. 2. Spectral functions of two-particle excitations in equilibrium SC phase (a), CDW phase (b), and in non-equilibrium after quenching from the CDW ground state into the SC phase evaluated at time $t = 15$ (c). Note that only regions with significant spectral weight are displayed.

as the differential spectral function, where we have introduced a spectral broadening $\eta = 0.1$ [23]. Note that here we explicitly do not restrict ourselves to single-electron excitations, but also study processes that may excite double occupations, i.e., doublons. This can be related to ongoing experiments [61], in which photoemission of pairs of electrons is studied, and is theoretically corroborated in a BCS-type picture [60]. Fig. 2 displays the spectral functions for double occupations $S_{\hat{d}}(q, \omega, \Delta t)$ for both equilibrium phases (SC and CDW) and after the quench. We obtain a clear accumulation of weight at $q = 0$ in the postquench state, which renders the result similar to the one of the SC ground state displayed. This is the central statement of this Letter: A (quasi-)condensate of s-wave (Cooper-)pairs seems to form after the quench, which is clearly detectable in $S_{\hat{d}}(q, \omega, \Delta t)$, and which has a striking similarity to the spectral function in the SC ground state. We emphasize that this coherence between the charges is dynamically created after the quench, as seen in the comparison with Fig. 2b, which shows dispersive, incoherent doublons. We observe similar behavior in the corresponding pairing spectral function of the t - J_{\perp} model [53], so that we expect this to be a generic feature, at least for quenches to SC phases.

Current tr-ARPES experiments usually investigate the time evolution of the spectral functions for single-electron excitations $S_{\hat{c}}(q, \omega, \Delta t)$, which we show in Fig. 3. The signatures to discriminate the SC phase from the CDW phase are not as prominent as for the double occupations. Nevertheless, we find that in the SC ground

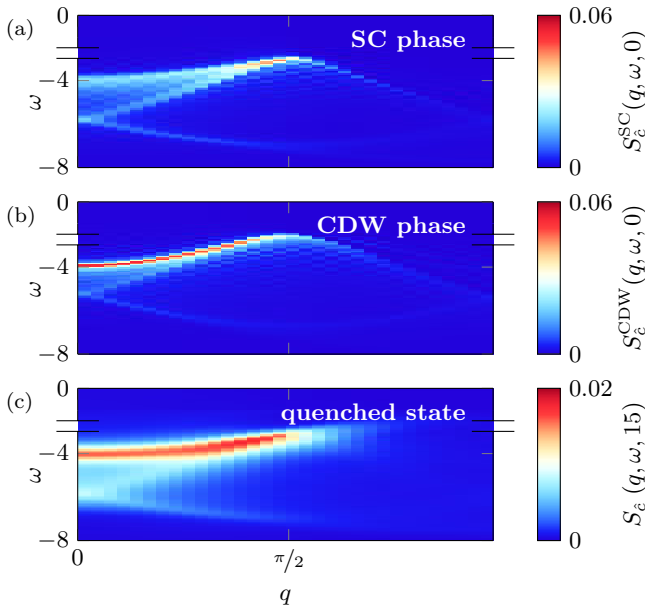


FIG. 3. Spectral functions of single-particle excitations in equilibrium SC phase (a), CDW phase (b), and in non-equilibrium after quenching from the CDW ground state into the SC phase evaluated at time $t = 15$ (c). Note that only regions with significant spectral weight are displayed.

state (Fig. 3a) there is a shift of spectral weight towards $q = \pi/2$. This is to be contrasted with the distribution of weights in the CDW ground state, where the maximum value is at $q = 0$. Comparing to the spectral function after the quench (Fig. 3c), a weak transfer of spectral weight from $q = 0$ towards $q = \pi/2$ can be identified. However, from the numerical data it is not possible to clearly identify this as a signal for a (transient) SC phase. Note that the observed behavior is not reproduced for a quench within the CDW phase, as the two-electron excitations do not show a sharp signal at small momenta, indicating the absence of a transient SC phase there [53].

Correlation Matrices Now we turn to the question on how to further characterize the observed transient state. To do so, we attempt a standard analysis for the investigation of LRO in equilibrium systems and apply it to the present non-equilibrium situation. In Ref. 58, Onsager and Penrose suggest to detect off-diagonal LRO by determining the eigenvalues λ_ν of single-particle correlation matrices,

$$\chi_{\hat{O}} = \sum_{i,j} \mathbf{e}_i \langle \psi | \hat{O}_i^\dagger \hat{O}_j | \psi \rangle \mathbf{e}_j^t \equiv \sum_{i,j} \mathbf{e}_i \chi_{\hat{O}}(i, j) \mathbf{e}_j^t, \quad (4)$$

i.e., $\chi_{\hat{O}} \mathbf{v}_\nu = \lambda_\nu \mathbf{v}_\nu$ [68]. This concept was generalized by Yang [69] to include also two-particle correlation matrices to describe superconductivity. The correlation matrix determines the order parameter if the dominating eigenvalue scales extensively in the system size $\lim_{L \rightarrow \infty} \frac{\lambda_L}{L} \rightarrow \mathcal{O}(1)$, which also implies an extensive separation of the dominating eigenvalue λ_L from the bulk [53].

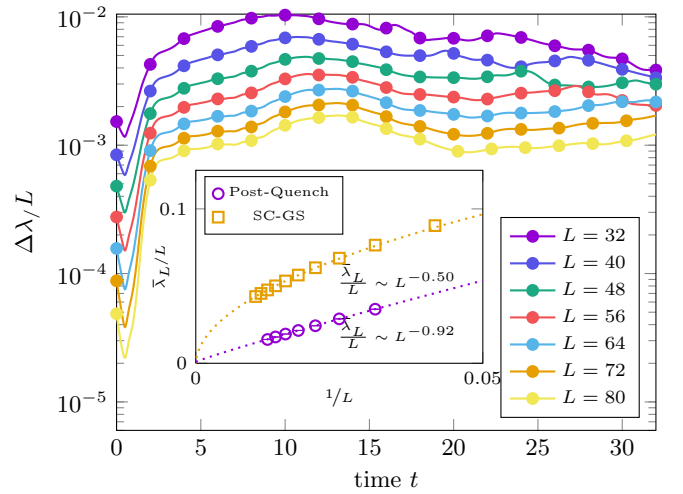


FIG. 4. Separation of largest natural orbital occupation $\Delta\lambda/L = \frac{\lambda_L - \lambda_{L-1}}{L}$ during time evolution after quench for various system sizes. The inset shows the scaling behavior of the normalized dominating eigenvalue $\bar{\lambda}_L/L$ with system size L .

Due to the Mermin-Wagner-Hohenberg theorem [31–33], in 1D and in equilibrium, for pair formation only quasi-long-range order (qLRO) can be realized, which translates to a SC order parameter vanishing in the thermodynamic limit. Here, we studied the time evolution of the correlation matrix $\chi_{\hat{d}}(i, j) = \langle \psi(t) | \hat{d}_i^\dagger \hat{d}_j | \psi(t) \rangle$, which provides the SC order parameter. Figure 4 shows the difference between the two largest eigenvalues $\Delta\lambda/L = \frac{\lambda_L - \lambda_{L-1}}{L}$ as a function of time. At later times we find this separation to be about an order of magnitude larger than in the initial state. We have estimated the saturation values of the dominating eigenvalue by averaging over the accessible time scales, in which we assumed quasi-stationarity, $\bar{\lambda}_L = \frac{1}{t_1 - t_0} \sum_{t=t_0}^{t_1} \lambda_L(t)$ with $t_0 = 10, t_1 = 32$. In the inset of Fig. 4, we compare the scaling behavior to the one of the SC ground state, where $\bar{\lambda}_L/L \sim L^{-0.50} = 1/\sqrt{L}$ is realized, with saturation value $\beta_{\text{SC}} = -1 \times 10^{-3} \approx 0$, as expected. After the quench, the scaling is best described by fitting the asymptotic behavior with $\bar{\lambda}_L/L \sim L^{-0.92} \sim 1/L$, and in this case we extracted a value $\beta = 9 \times 10^{-4}$, whose magnitude is even smaller than the one obtained in equilibrium, and hence zero within the error bars of our scaling analysis. This scaling to zero indicates that no LRO is obtained on the time scales investigated but cannot be excluded for later times [70, 71].

Conclusion and Outlook Our results for the differential optical conductivity in the extended Hubbard model after a quench indicate that the enhancement of $\sigma_2(\omega, \Delta t)$ in the low-frequency regime does not suffice to uniquely identify SC: The currents induced by a probe pulse cannot unambiguously be identified as supercurrents. In contrast, the pairing spectral function shows a

clear accumulation of weights at $q \rightarrow 0$, which is absent in our initial state, but present in the SC ground state. This provides stronger evidence for the formation of a non-equilibrium SC state than the reflectivity measurements.

Our study indicates that reflectivity measurements need to be complemented by tr-ARPES-type experiments in future investigations. Readily available tr-ARPES setups measure the single-particle spectral function, which shows a shift of weights towards the SC state. We propose to also investigate the time evolution of pairing spectral functions, which provide the clearest evidence for the formation of a transient SC state. Our work therefore supplies an important theoretical result for the growing field of double photoemission spectroscopy.

Acknowledgements We thank B. Lenz, L. Cevolani, K. Harms, N. Abeling, F. Heidrich-Meisner, S. Kaiser, G. Uhrig, and K. Schönhammer for insightful discussions. B.F. and D.M. thank the Max Planck-UBC-UTokyo Center for Quantum Materials for financial support. T.K.'s contribution was partially funded through an ERC Starting Grant from the European Union's Horizon 2020 research and innovation program under grant agreement No. 758935. We acknowledge financial support by the Deutsche Forschungsgemeinschaft (DFG) through SFB/CRC1073 (projects B03 and B07) and Research Unit FOR 1807 (project P7), and TU Clausthal for providing access to the Nuku computational cluster as well as the GWDG for providing HPC resources. This work was supported in part by the Los Alamos National Laboratory LDRD Program. S.P., T.K., and S.R.M. thank MPI-FKF for their hospitality.

-
- [1] J. G. Bednorz and K. A. Müller, *Zeitschrift für Physik B Condensed Matter* **64**, 189 (1986).
- [2] M. K. Wu, J. R. Ashburn, C. J. Torng, P. H. Hor, R. L. Meng, L. Gao, Z. J. Huang, Y. Q. Wang, and C. W. Chu, *Phys. Rev. Lett.* **58**, 908 (1987).
- [3] E. Dagotto, *Rev. Mod. Phys.* **66**, 763 (1994).
- [4] P. A. Lee, N. Nagaosa, and X.-G. Wen, *Rev. Mod. Phys.* **78**, 17 (2006).
- [5] M. Först, A. Frano, S. Kaiser, R. Mankowsky, C. R. Hunt, J. J. Turner, G. L. Dakovski, M. P. Minitti, J. Robinson, T. Loew, M. Le Tacon, B. Keimer, J. P. Hill, A. Cavalleri, and S. S. Dhesi, *Phys. Rev. B* **90**, 184514 (2014).
- [6] R. Mankowsky, A. Subedi, M. Frst, S. O. Mariager, M. Chollet, H. T. Lemke, J. S. Robinson, J. M. Glownia, M. P. Minitti, A. Frano, M. Fechner, N. A. Spaldin, T. Loew, B. Keimer, A. Georges, and A. Cavalleri, *Nature* **516**, 71 (2014).
- [7] W. Hu, S. Kaiser, D. Nicoletti, C. R. Hunt, I. Gierz, M. C. Hoffmann, M. Le Tacon, T. Loew, B. Keimer, and A. Cavalleri, *Nature Materials* **13**, 705 (2014).
- [8] C. R. Hunt, D. Nicoletti, S. Kaiser, D. Präpper, T. Loew, J. Porras, B. Keimer, and A. Cavalleri, *Phys. Rev. B* **94**, 224303 (2016).
- [9] M. Mitranò, A. Cantaluppi, D. Nicoletti, S. Kaiser, A. Perucchi, S. Lupi, P. Di Pietro, D. Pontiroli, M. Ricc, S. R. Clark, D. Jaksch, and A. Cavalleri, *Nature* **530**, 461 (2016).
- [10] M. Frst, C. Manzoni, S. Kaiser, Y. Tomioka, Y. Tokura, R. Merlin, and A. Cavalleri, *Nature Physics* **7**, 854 (2011).
- [11] D. Fausti, R. I. Tobey, N. Dean, S. Kaiser, A. Dienst, M. C. Hoffmann, S. Pyon, T. Takayama, H. Takagi, and A. Cavalleri, *Science* **331**, 189 (2011).
- [12] S. Kaiser, C. R. Hunt, D. Nicoletti, W. Hu, I. Gierz, H. Y. Liu, M. Le Tacon, T. Loew, D. Haug, B. Keimer, and A. Cavalleri, *Phys. Rev. B* **89**, 184516 (2014).
- [13] M. Buzzi, D. Nicoletti, M. Fechner, N. Tancogne-Dejean, M. A. Sentef, A. Georges, M. Dressel, A. Henderson, T. Siegrist, J. A. Schlueter, K. Miyagawa, K. Kanoda, M. S. Nam, A. Ardavan, J. Coulthard, J. Tindall, F. Schlawin, D. Jaksch, and A. Cavalleri, arXiv e-prints arXiv:2001.05389 (2020).
- [14] R. Singla, G. Cotugno, S. Kaiser, M. Först, M. Mitranò, H. Y. Liu, A. Cartella, C. Manzoni, H. Okamoto, T. Hasegawa, S. R. Clark, D. Jaksch, and A. Cavalleri, *Phys. Rev. Lett.* **115**, 187401 (2015).
- [15] M. Eckstein, M. Kollar, and P. Werner, *Phys. Rev. B* **81**, 115131 (2010).
- [16] D. M. Kennes, E. Y. Wilner, D. R. Reichman, and A. J. Millis, *Phys. Rev. B* **96**, 054506 (2017).
- [17] Y. Wang, M. Claassen, B. Moritz, and T. P. Devereaux, *Phys. Rev. B* **96**, 235142 (2017).
- [18] N. Bittner, T. Tohyama, S. Kaiser, and D. Manske, *Journal of the Physical Society of Japan* **88**, 044704 (2019).
- [19] B. Fauseweh, L. Schwarz, N. Tsuji, N. Cheng, N. Bittner, H. Krull, M. Berciu, G. S. Uhrig, A. P. Schnyder, S. Kaiser, and D. Manske, *Nat. Commun.* **11**, 287 (2020).
- [20] L. Schwarz, B. Fauseweh, and D. Manske, arXiv e-prints arXiv:2002.05904 (2020).
- [21] S. R. White, *Phys. Rev. Lett.* **69**, 2863 (1992).
- [22] U. Schollwöck, *Annals of Physics* **326**, 96 (2011).
- [23] S. Paecel, T. Köhler, A. Swoboda, S. R. Manmana, U. Schollwöck, and C. Hubig, *Annals of Physics* **411**, 167998 (2019).
- [24] A. Damascelli, Z. Hussain, and Z.-X. Shen, *Rev. Mod. Phys.* **75**, 473 (2003).
- [25] A. Damascelli, *Physica Scripta* **T109**, 61 (2004).
- [26] D. Lynch and C. Olson, *Photoemission Studies of High-Temperature Superconductors, Cambridge Studies in Low Temperature Physics* (Cambridge University Press, Cambridge, 2005).
- [27] M. Eckstein and M. Kollar, *Phys. Rev. B* **78**, 245113 (2008).
- [28] J. K. Freericks, H. R. Krishnamurthy, and T. Pruschke, *Phys. Rev. Lett.* **102**, 136401 (2009).
- [29] M. Ligges, I. Avigo, D. Golež, H. U. R. Strand, Y. Beyazit, K. Hanff, F. Diekmann, L. Stojchevska, M. Källäne, P. Zhou, K. Rossnagel, M. Eckstein, P. Werner, and U. Bovensiepen, *Phys. Rev. Lett.* **120**, 166401 (2018).
- [30] Y. Wang, M. Claassen, C. D. Pemmaraju, C. Jia, B. Moritz, and T. P. Devereaux, *Nature Reviews Materials* **1** (2018).
- [31] N. D. Mermin and H. Wagner, *Phys. Rev. Lett.* **17**, 1133 (1966).

- [32] N. D. Mermin and H. Wagner, *Phys. Rev. Lett.* **17**, 1307 (1966).
- [33] P. C. Hohenberg, *Phys. Rev.* **158**, 383 (1967).
- [34] J. Voit, *Rep. Prog. Phys.* **58**, 977 (1995).
- [35] J. Voit, *Phys. Rev. B* **45**, 4027 (1992).
- [36] E. Jeckelmann, *Phys. Rev. Lett.* **89**, 236401 (2002).
- [37] M. Tsuchiizu and A. Furusaki, *Phys. Rev. Lett.* **88**, 056402 (2002).
- [38] A. W. Sandvik, L. Balents, and D. K. Campbell, *Phys. Rev. Lett.* **92**, 236401 (2004).
- [39] S. Ejima and S. Nishimoto, *Phys. Rev. Lett.* **99**, 216403 (2007).
- [40] F. Hofmann and M. Potthoff, *Phys. Rev. B* **85**, 205127 (2012).
- [41] K. A. Chao, J. Spalek, and A. M. Oles, *Journal of Physics C: Solid State Physics* **10**, L271 (1977).
- [42] P. W. Anderson, *Science* **235**, 1196 (1987).
- [43] F. C. Zhang and T. M. Rice, *Phys. Rev. B* **37**, 3759 (1988).
- [44] A. Moreno, A. Muramatsu, and S. R. Manmana, *Phys. Rev. B* **83**, 205113 (2011).
- [45] A. V. Gorshkov, S. R. Manmana, G. Chen, J. Ye, E. Demler, M. D. Lukin, and A. M. Rey, *Phys. Rev. Lett.* **107**, 115301 (2011).
- [46] S. R. Manmana, M. Möller, R. Gezzi, and K. R. A. Hazard, *Phys. Rev. A* **96**, 043618 (2017).
- [47] J. Hubbard, *Proceedings of the Royal Society of London A: Mathematical, Physical and Engineering Sciences* **276**, 238 (1963).
- [48] M. C. Gutzwiller, *Phys. Rev. Lett.* **10**, 159 (1963).
- [49] J. Kanamori, *Progress of Theoretical Physics* **30**, 275 (1963).
- [50] F. H. L. Essler, H. Frahm, F. Göhmann, A. Klümper, and V. E. Korepin, *The One-Dimensional Hubbard Model* (Cambridge University Press, Cambridge, 2005).
- [51] J. Eisert, M. Friesdorf, and C. Gogolin, *Nature Physics* **11**, 124 (2015).
- [52] N. Bittner, *Novel NonEquilibrium Dynamics in Superconductors: Induced Superconductivity and Higgs Modes*, PhD thesis, Freie Universität Berlin, 2017.
- [53] See Supplemental Material at [URL will be inserted by publisher] for a detailed description of the definition and numerical details of the spectral functions, (non-)thermal properties of the postquench state, scaling analysis of the eigenvalues of the correlation matrices (natural orbitals), and results for the $t - J_{\perp}$ model.
- [54] Y. Nomura, S. Sakai, M. Capone, and R. Arita, *Science Advances* **1**, (2015).
- [55] J. Haegeman, C. Lubich, I. Oseledets, B. Vandereycken, and F. Verstraete, *Phys. Rev. B* **94**, 165116 (2016).
- [56] Z. Lenarčič, D. Golež, J. Bonča, and P. Prelovšek, *Phys. Rev. B* **89**, 125123 (2014).
- [57] C. Shao, T. Tohyama, H.-G. Luo, and H. Lu, *Phys. Rev. B* **93**, 195144 (2016).
- [58] O. Penrose and L. Onsager, *Phys. Rev.* **104**, 576 (1956).
- [59] M. Rigol and A. Muramatsu, *Phys. Rev. A* **70**, 031603 (2004).
- [60] K. A. Kouzakov and J. Berakdar, *Phys. Rev. Lett.* **91**, 257007 (2003).
- [61] A. Trütschler, M. Huth, C.-T. Chiang, R. Kamrla, F. O. Schumann, J. Kirschner, and W. Widdra, *Phys. Rev. Lett.* **118**, 136401 (2017).
- [62] C. Stahl and M. Eckstein, *Phys. Rev. B* **99**, 241111 (2019).
- [63] T. Giamarchi, *Quantum Physics in One Dimension*, Vol. 121 of *International Series of Monographs on Physics* (Oxford University Press, Oxford, 2004).
- [64] The operators S_j^{\pm} are the usual $S - 1/2$ ladder operators on site j . Note that double occupancies are forbidden in the t - J model.
- [65] For the width of the probe pulse we chose $\tau = 0.05$ throughout this letter.
- [66] D. R. Hofstadter, *Phys. Rev. B* **14**, 2239 (1976).
- [67] In [57] the non-equilibrium response function is obtained by considering the Fourier transform of the difference $j(t, \Delta t) - j_0(t)$ with $j_0(t)$ the current without probe pulse. As in our quench protocol without probe pulse there is always $j_0(t) \equiv 0$ we drop this term for brevity.
- [68] We use the bold symbol \mathbf{e}_j to denote canonical unit vectors.
- [69] C. N. Yang, *Rev. Mod. Phys.* **34**, 694 (1962).
- [70] Y. Lemonik and A. Mitra, *Phys. Rev. B* **96**, 104506 (2017).
- [71] Y. Lemonik and A. Mitra, *Phys. Rev. Lett.* **121**, 067001 (2018).

Supplementary Material for “Detecting superconductivity out-of-equilibrium”

S. Paegel,^{1,2} B. Fauseweh,^{3,4} A. Osterkorn,² T. Köhler,^{5,2} D. Manske,³ and S.R. Manmana²

¹Fakultät für Physik, Ludwig-Maximilians-Universität München, D-80333 München, Germany

²Institut für Theoretische Physik, Georg-August-Universität Göttingen, D-37077 Göttingen, Germany

³Max-Planck-Institut für Festkörperforschung, Heisenbergstraße 1, D-70569 Stuttgart, Germany

⁴Theoretical Division, Los Alamos National Laboratory, Los Alamos, New Mexico 87545, USA

⁵Department of Physics and Astronomy, Uppsala University, Box 516, S-751 20 Uppsala, Sweden

SPECTRAL FUNCTION

General theory We defined the differential spectral function $S_{\hat{O}}(q, \omega, \Delta t)$ by the power spectrum in momentum space of the propagator of the operators \hat{O}_j

$$S_{\hat{O}}(q, \omega, \Delta t) = \int_{-\infty}^{\infty} \frac{dt}{2\pi} e^{i\omega t} C_{\hat{O}}(q, t, \Delta t), \quad (1)$$

$$\begin{aligned} C_{\hat{O}}(q, t, \Delta t) &= \frac{1}{L} \sum_{r_{ij}} e^{-iqr_{ij}} \langle \psi(\Delta t) | \hat{O}_i^\dagger(t) \hat{O}_j(0) | \psi(\Delta t) \rangle \\ &= \langle \hat{O}_q^\dagger(t) \hat{O}_q(0) \rangle_{\Delta t}, \end{aligned} \quad (2)$$

where we defined $r_{ij} = r_i - r_j = (i - j) \cdot a$ in terms of the lattice spacing a and abbreviated the expectation values at time delay Δt by $\langle \psi(\Delta t) | \dots | \psi(\Delta t) \rangle \equiv \langle \dots \rangle_{\Delta t}$. The \hat{O}_i 's are operators obeying canonical (anti-)commutation relations $[\hat{O}_i, \hat{O}_j^\dagger]_{\pm} \propto \delta_{ij}$ and so do their Fourier transformed counterparts

$$\hat{O}_q = \frac{1}{\sqrt{L}} \sum_{r_i} e^{-iqr_i} \hat{O}_i, \quad [\hat{O}_q, \hat{O}_k^\dagger]_{\pm} \propto \delta_{qk}. \quad (3)$$

The differential spectral function is reformulated to simplify the numerical evaluation:

$$S_{\hat{O}}(q, \omega, \Delta t) = \int_0^{\infty} \frac{dt}{2\pi} [e^{i\omega t} C_{\hat{O}}(q, t, \Delta t) + e^{-i\omega t} C_{\hat{O}}(q, -t, \Delta t)] = \int_0^{\infty} \frac{dt}{2\pi} [e^{i\omega t} C_{\hat{O}}(q, t, \Delta t) + e^{-i\omega t} C_{\hat{O}}^*(q, t, \Delta t)], \quad (4)$$

where we assumed a (quasi-)steady state to exploit time translational invariance to shift the argument: $\langle \hat{O}_q^\dagger(-t) \hat{O}_q(0) \rangle = \langle \hat{O}_q^\dagger(0) \hat{O}_q(t) \rangle = \langle \hat{O}_q^\dagger(t) \hat{O}_q(0) \rangle^*$. Thus, we can evaluate the time integral by taking the real part of the Fourier transformation and restrict the integration domain to $t \geq 0$. Note that in order to discretize the Fourier transformation, we defined the limit as

$$S_{\hat{O}}(q, \omega, \Delta t) = \lim_{T \rightarrow \infty} \frac{1}{T} \int_{-T/2}^{T/2} dt e^{i\omega t} C_{\hat{O}}(q, t, \Delta t). \quad (5)$$

Using Eq. (4), we thus numerically evaluated the Fourier transformation via

$$S_{\hat{O}}(q, \omega_n, \Delta t) = \frac{\delta}{T} \text{Re} \sum_{m=0}^{N_T-1} e^{i\omega_n t_m} C_{\hat{O}}(q, t_m, \Delta t), \quad (6)$$

with discretized frequencies $\omega_n = n \frac{2\pi}{T}$ ($n = 0, \dots, N_T - 1$), $t_m = m\delta$ and the summation range fixed by the time step $\delta = T/N_T$. Note that this way we only obtain the positive frequency part which we accounted for by shifting the time arguments, relabeling $t_m \rightarrow t_m - T/2 \Rightarrow \omega_n \rightarrow \omega_n - \pi/T$.

Numerical technique We calculated the time-evolution of the lesser Greens function

$$C_{\hat{O}}(j, t, \Delta t) = \langle \psi(\Delta t) | \hat{O}_j^\dagger(t) \hat{O}_{L/2}(0) | \psi(\Delta t) \rangle, \quad (7)$$

by representing the states and operators in the matrix-product state (MPS) and matrix-product operator (MPO) framework [1–3]. Within this framework the wavefunctions $|\psi\rangle = \sum_{\sigma_1, \dots, \sigma_L} \psi_{\sigma_1, \dots, \sigma_L} |\sigma_1, \dots, \sigma_L\rangle$ are approximated in terms of a tensor-network decomposition of the coefficients of the states

$$\psi_{\sigma_1, \dots, \sigma_L} = \sum_{\{\alpha_j\}} M_{\alpha_1}^{\sigma_1} M_{\alpha_1, \alpha_2}^{\sigma_2} \dots M_{\alpha_{L-2}, \alpha_{L-1}}^{\sigma_{L-1}} M_{\alpha_{L-1}}^{\sigma_L}, \quad (8)$$

and a similar expansion exists for operators. The range of the so-called bond indices α_j is usually known as bond dimension of the MPS and is closely related to the von-Neumann entanglement entropy S_N of the state for a bipartition of the Hilbert space at bond $(j - 1, j)$. It can be shown that by fixing the maximal bond dimension to a certain value m states can be faithfully approximated as long as their bipartite entanglement entropy is not significantly exceeding values of $\log_\sigma(m)$ where σ denotes the dimension of the local degrees of freedom, i.e., the Hubbard ($\sigma = 4$) or the t - J -basis ($\sigma = 3$) of spin-1/2 fermions in the systems treated by us. This condition is usually fulfilled for ground states of gapped systems in one dimension [4, 5] but is no longer valid out-of-equilibrium. In order to evaluate the time-dependent Greens function we used the Schrödinger picture to decompose the scalar

product

$$C_{\hat{O}}(j, t, \Delta t) \equiv \langle \psi(t, \Delta t) | \hat{O}_j^\dagger | \phi(t, \Delta t) \rangle$$

$$|\psi(t, \Delta t)\rangle = \hat{U}(t) |\psi(\Delta t)\rangle \quad (9)$$

$$|\phi(t, \Delta t)\rangle = \hat{U}(t) \hat{O}_{L/2}(0) |\psi(\Delta t)\rangle \quad (10)$$

and calculated the time evolutions independently. The maximally achieved time scales when evaluating the time evolution of the lesser Greens function were $t = 32$. For determining the time evolution itself we used a hybrid version of the time-dependent variational principle (TDVP) algorithm [3, 6] where we combined a two-site

solver in the initial stage of the time evolution to grow the bond dimensions until the maximum value was reached on all bonds. Then we switched to a faster single-site solver of the local TDVP equations to continue the time evolution.

The nature of the problem demands a high numerical effort to obtain the results presented in this letter. Therefore, we used a state-of the art implementation exploiting $U(1)$ -symmetries [7].

Useful identities Integrating over the frequency domain, the propagator fulfills

$$\int_{-\infty}^{\infty} d\omega \int_{-\infty}^{\infty} \frac{dt}{2\pi} e^{i\omega t} C_{\hat{O}}(q, t, \Delta t) = \int_{-\infty}^{\infty} d\omega \int_{-\infty}^{\infty} \frac{dt}{2\pi} e^{i\omega t} \sum_{n,m} \langle \psi(\Delta t) | n \rangle \langle n | \hat{O}_q^\dagger(t) | m \rangle \langle m | \hat{O}_q | \psi(\Delta t) \rangle = \langle \hat{O}_q^\dagger \hat{O}_q \rangle_{\Delta t}, \quad (11)$$

which implies the sum rule

$$2 \sum_q \int_0^\infty d\omega \operatorname{Re} S_{\hat{O}}(q, \omega, \Delta t) = \sum_q \langle \hat{O}_q^\dagger \hat{O}_q \rangle_{\Delta t}. \quad (12)$$

Thus, for $\hat{O}_i = \hat{c}_{i,\sigma}$ this yields the total number of particles with local spin projection σ , while for $\hat{O}_i = \hat{d}_i$ we expect the overall number of doublons in the system. Note that the overall doublon occupation $\hat{D} = \sum_i \hat{d}_i^\dagger \hat{d}_i$ in general is not conserved by \hat{H} . However, the sum rule holds at each time delay Δt . In particular, if the correlation function is invariant under time-translations on some time interval I , \hat{D} will be conserved on I .

NATURAL ORBITALS

General Theory We consider a correlation matrix for some local observable \hat{O}_j

$$\chi_{\hat{O}}(i, j) = \langle \psi | \hat{O}_i^\dagger \hat{O}_j | \psi \rangle. \quad (13)$$

Then, off-diagonal long-range order (LRO) in the thermodynamic limit is defined according to

$$\lim_{|i-j| \rightarrow \infty} \chi_{\hat{O}}(i, j) > 0, \quad (14)$$

i.e., the correlation function $\chi_{\hat{O}}(i, j)$ saturates at a finite value for arbitrary large separations $|i-j|$. In the following we will briefly summarize the discussion on natural orbitals (see, for instance, [8, 9]) to review the tools exploited in the main text to identify off-diagonal LRO.

For a finite system with L lattice sites, $\chi_{\hat{O}}(i, j)$ is a Hermitian $L \times L$ matrix, which we can formally diagonalize to obtain real eigenvalues λ_ν and corresponding

eigenvectors \mathbf{v}_ν . Expanding $\chi_{\hat{O}}(i, j)$ as matrix $\chi_{\hat{O}}$ in its eigenbasis, we can write

$$\chi_{\hat{O}} = \sum_\nu \mathbf{v}_\nu \langle \psi | \underbrace{\left(\sum_i v_{\nu,i}^* \hat{O}_i^\dagger \right) \left(\sum_j v_{\nu,j} \hat{O}_j \right)}_{\lambda_\nu} | \psi \rangle \mathbf{v}_\nu^\dagger. \quad (15)$$

Introducing field operators $\hat{\eta}_\nu = \sum_i v_{\nu,i} \hat{O}_i$, their squared expectation values are related to the eigenvalues λ_ν of $\chi_{\hat{O}}$

$$\mathbf{v}_\nu^\dagger \chi_{\hat{O}} \mathbf{v}_\nu = \langle \psi | \hat{\eta}_\nu^\dagger \hat{\eta}_\nu | \psi \rangle = \lambda_\nu \geq 0, \quad (16)$$

i.e., the eigenvalues are strictly positive. If we impose $[\hat{O}_i, \hat{O}_j^\dagger]_\epsilon = \delta_{ij}$ with $\epsilon = \pm 1$ choosing between the commutator (+1) and anticommutator (-1), it follows that

$$[\hat{\eta}_\nu, \hat{\eta}_\mu^\dagger]_\epsilon = \sum_{i,j} [\hat{O}_i, \hat{O}_j^\dagger]_\epsilon v_{\nu,i} v_{\mu,j}^* = \delta_{\nu\mu}. \quad (17)$$

This suggests to call the eigenvectors \mathbf{v}_ν natural orbitals and the eigenvalues natural orbital occupations λ_ν of the correlation matrix $\chi_{\hat{O}}$.

The existence of off-diagonal LRO can now be related to properties of the natural orbitals. To see this, note that due to the canonical commutator relations of \hat{O}_j the trace over $\chi_{\hat{O}}$ corresponds to the total occupation $N_{\hat{O}} = \sum_j \langle \hat{n}_j \rangle \equiv \sum_j \langle \hat{O}_j^\dagger \hat{O}_j \rangle$ of the single particle states generated by the \hat{O}_j 's. If we assume that there is a natural orbital \mathbf{v}_L that is macroscopically occupied, i.e., $\lambda_L/N_{\hat{O}} \sim \mathcal{O}(1)$, it is instructive to pull out this contribution from the sum in Eq. (15). Written out component-

wise, we find

$$\chi_{\hat{O}}(i, j) = \lambda_L v_{L,i} v_{L,j}^* + \sum_{\nu < L} \lambda_\nu v_{\nu,i} v_{\nu,j}^*. \quad (18)$$

The natural orbitals are normalized so that in general the components fulfill $v_{\nu,j} \sim 1/\sqrt{L}$. Therefore, an extensively scaling natural orbital occupation λ_L yields a dominating leading summand in the above expansion of the correlation matrix, while the remaining summands are suppressed as $1/L$. In this situation, for increasing system sizes L the correlation matrix is well approximated by neglecting the latter,

$$\chi_{\hat{O}}(i, j) = \lambda_L v_{L,i} v_{L,j}^* + \mathcal{O}(1/L) \approx \lambda_L v_{L,i} v_{L,j}^*. \quad (19)$$

The correlation matrix obtained this way factorizes in the spatial components (i, j) . Since, in a state with explicitly broken symmetry with respect to \hat{O}_j , one expects $\langle \hat{O}_j \rangle \neq 0$, this permits to identify

$$\chi_{\hat{O}}(i, j) = \langle \hat{O}_i^\dagger \rangle \langle \hat{O}_j \rangle \equiv \sqrt{\lambda_L} v_{L,i} \sqrt{\lambda_L} v_{L,i}^*, \quad (20)$$

so that $\sqrt{\lambda_L} v_{L,j}$ constitutes the microscopic local order parameter.

Quasi-long-range order and error estimates In the following paragraphs, we focus on our results for the correlation matrix of double occupancies $\chi_{\hat{d}}(i, j) = \langle \psi | \hat{d}_i^\dagger \hat{d}_j | \psi \rangle$. The problem under consideration is one-dimensional so that due to the Mermin-Wagner-Hohenberg theorem [10–12] at least in the ground state there can be quasi-long-range order (qLRO) only. This translates to a still extensively scaling, dominating natural orbital but with vanishing value in the thermodynamic limit. In the case of a non-interacting gas of hardcore bosons on a lattice, it is well-known [13, 14] that

$$\frac{\lambda_{\bar{\nu}}}{L} \stackrel{L \rightarrow \infty}{\sim} \frac{A}{\sqrt{L}} + \beta_{\text{SC}} \quad (21)$$

with $\beta_{\text{SC}} \equiv 0$, which is in excellent agreement with our ground-state calculations in the superconducting phase at $U = -4, V = -1/4$ and $\hat{O}_j = \hat{d}_j$. We performed a finite size scaling of the eigenvalue of the dominant natural orbital by fitting the function $\frac{\lambda_{\bar{\nu}}}{L}$ over $L^{-\gamma}$ with $\gamma = 0.50$ in the superconducting ground state. The obtained value for the order parameter is $\beta_{\text{SC}} = -1 \times 10^{-3}$, which we used to gauge the precision of our method to be $\delta \sim \mathcal{O}(10^{-3})$. In the non-equilibrium situation, we time-averaged the dominating natural orbital for times $t_0 \geq t_0$ via

$$\bar{\lambda}_{\bar{\nu}} = \frac{1}{t_1 - t_0} \sum_n \lambda_{\bar{\nu}}(t_0 + n\delta), \quad (22)$$

with δ being the time step of the time-evolution scheme and with $t_0 = 10, t_1 = 32$. Performing the finite-size analysis, we found the data to be best described by a scaling $\sim \alpha \cdot L^{-\gamma} + \beta_{\text{SC}}$ with $\gamma = 0.92$ and $\beta_{\text{SC}} = 9 \cdot 10^{-4}$. Within the error bounds deduced from the ground-state analysis, this implies $\beta_{\text{SC}} \equiv 0$, and hence no LRO.

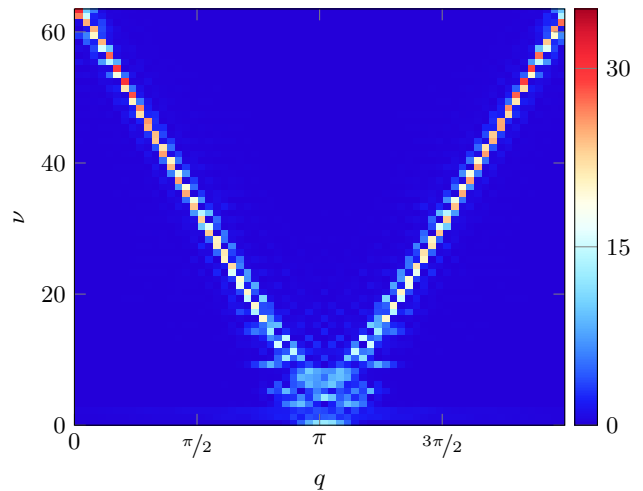


FIG. 1. Absolute value of the Fourier transform of the natural orbitals $\tilde{\mathbf{v}}_\nu(t = 32)$ after quenching from the CDW to the SC phase.

Momentum space To complete the discussion, we calculated the Fourier transformation of the natural orbitals $\tilde{v}_{\nu,q} = \sum_j v_{\nu,j} e^{iqj}$. As shown in Fig. 1, the Fourier modes $\tilde{\mathbf{v}}_\nu$ are nearly diagonal in k -space, i.e., the correlation matrix is approximately diagonalized by a Fourier transformation and the dominating natural orbital (NO) is characterized by a mode with $q = 0$. The off-diagonal contributions around $q = \pi$ arise from highly excited states (cf. the band spectral function in the main text). Inspecting their real-space distributions $|v_{\nu,j}|^2$ (not shown here) these are located near the boundaries so that we conjecture them to vanish in the thermodynamic limit. We observe these properties consistently for times $t > 4$ in all considered system sizes $L \in [32, 80]$.

J-QUENCH IN THE t - J_\perp CHAIN

Next to the extended Hubbard model, we considered the quench dynamics of the one-dimensional t - J_\perp Hamiltonian [15, 16]

$$\hat{H}_{t-J_\perp} = -t_{\text{hop}} \sum_{j,\sigma} \left(\hat{c}_{j,\sigma}^\dagger \hat{c}_{j+1,\sigma} + \text{H. c.} \right) + \frac{J_\perp}{2} \sum_j \left(\hat{S}_j^+ \hat{S}_{j+1}^- + \hat{S}_j^- \hat{S}_{j+1}^+ \right), \quad (23)$$

at filling $n = 0.2$. Its phase diagram [16] at $n = 0.2$ features a metallic (Luttinger liquid [17]) spin-density wave phase (SDW) at $J_\perp = 2t_{\text{hop}}$ and a spin-gapped singlet SC phase at $J_\perp = 6t_{\text{hop}}$. In the following, we compute the equilibrium one-particle as well as singlet-pair spectral functions at these two points in parameter space and also the non-equilibrium spectral functions at late times for a quench $J_\perp = 2t_{\text{hop}} \rightarrow J_\perp = 6t_{\text{hop}}$. Furthermore,

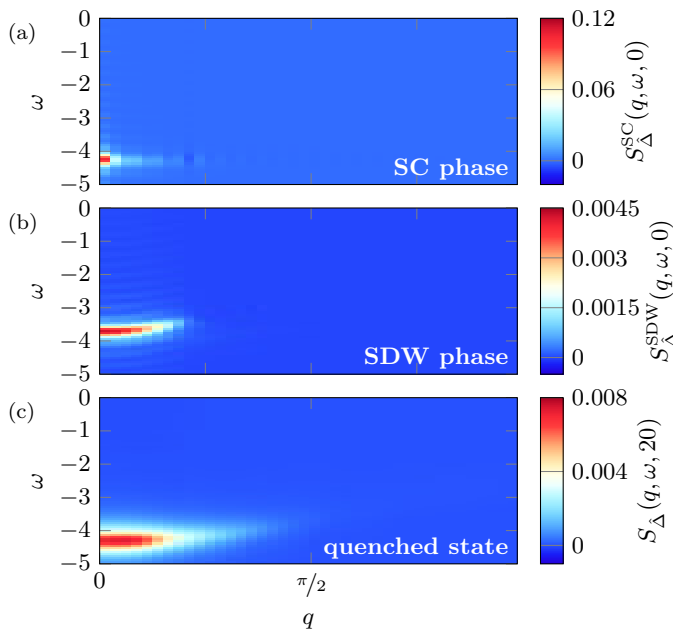


FIG. 2. Two-particle singlet spectral functions for the t - J_{\perp} model. Top: SC phase, middle: SDW phase, bottom: non-equilibrium state 20 time units after the quench.

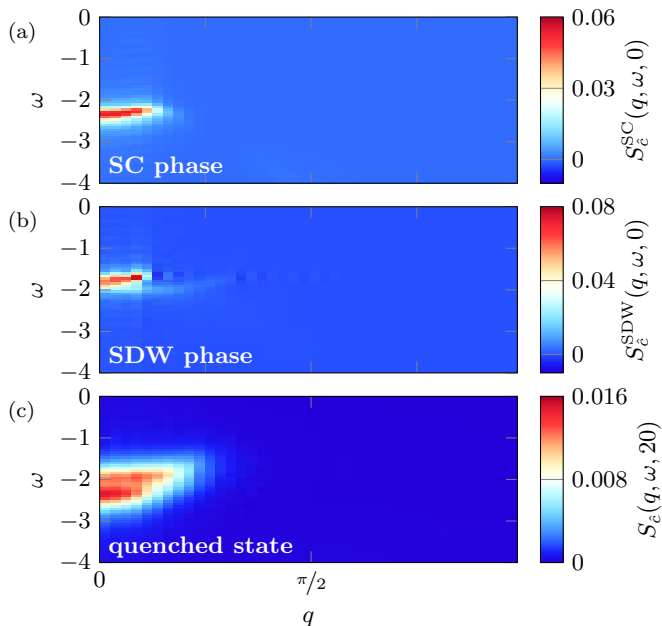


FIG. 3. Single-particle spectral functions for the t - J_{\perp} model. Top: SC phase, middle: SDW phase, bottom: non-equilibrium state 20 time units after the quench.

we discuss the time-evolution of the natural orbital occupations.

Spectral functions We consider the singlet-pair creation and annihilation operators

$$\hat{\Delta}_j^{(\dagger)} = \frac{1}{\sqrt{2}} \left(\hat{c}_{j,\uparrow}^{(\dagger)} \hat{c}_{j+1,\downarrow}^{(\dagger)} - \hat{c}_{j,\downarrow}^{(\dagger)} \hat{c}_{j+1,\uparrow}^{(\dagger)} \right) \quad (24)$$

and compute the two-particle spectral function according to Eqs. (1) and (6). The results are shown in Fig. 2 for the singlet-pair spectral function and in Fig. 3 for the one-particle spectral function (corresponding to the operators $c_{j,\uparrow}^{(\dagger)}$). A quasi-stationary state is estimated to be reached after about 20 time units. This is estimated from the time-evolution of the natural orbitals (cf. the corresponding section below).

The equilibrium two-particle SC spectral function shows a large weight at $q = 0$, whereas in the spin-density wave state it is much lower and a dispersion is visible. The peak amplitude of the non-equilibrium state is about doubled in comparison to the SDW and shifted towards the SC peak position. This is consistent with our findings in the extended Hubbard model in the main text where we find an increase of spectral weight around $q = 0$ in the postquench state (see Fig. 2c) and a shift of weight towards the SC state.

In the single-particle case the equilibrium spectral functions show the occupied states of a cosine dispersion (the unoccupied part of the spectrum is seen in the spectral function obtained from the greater Green's function). The spectral weights are of comparable amplitude but clearly differ in their ω -axis position. The non-equilibrium state is a kind of hybrid that contains weight around both the equilibrium branches.

Shift of the spectral peak As a guide to the eye, the peaks of the one- and two-particle spectral functions are replotted in Fig. 4. In addition to a slight increase in weight one can clearly see that the two-particle spectral peak in the post-quench state has shifted towards the superconducting peak position whereas in the one-particle case the picture is more complicated.

Hence, like in the main text the two-particle spectral function seems to be a more reliable indicator for the formation of transient superconducting spectral weights.

Natural orbitals At the end, analogous to the main text, we consider the question of whether true long-ranged order out-of-equilibrium is detectable from the correlation matrices. In Fig. 5 the time-dependent largest eigenvalue of the singlet-pair correlation matrix $\langle \hat{\Delta}_i^\dagger \hat{\Delta}_j \rangle_t$ is shown. As for the extended Hubbard model in the main text a saturation value can be made out after 20 time units. We use this as the criterion for the choice of the non-equilibrium reference state.

In order to perform a scaling analysis $\bar{\lambda}_m/L = \alpha \cdot L^{-\gamma} + \beta_{\text{SC}}$, we average over all largest natural orbitals for times $20 \leq t \leq 30$. The results shown in the inset of Fig. 5 yield a value of $\beta \approx -6 \cdot 10^{-5}$, such that $\beta_{\text{SC}} \approx 0$ within the estimated error bounds. This supports the conclusion that no true long-ranged order is realized in the transient state also for this model. The scaling exponent is found to be $\gamma \approx 1.12$ which is somewhat close to the scaling exponent of 0.92 found in the extended Hubbard model. Note that by definition $\gamma \leq 1$ so that the obtained scaling exponent has an error of $\approx 10\%$.

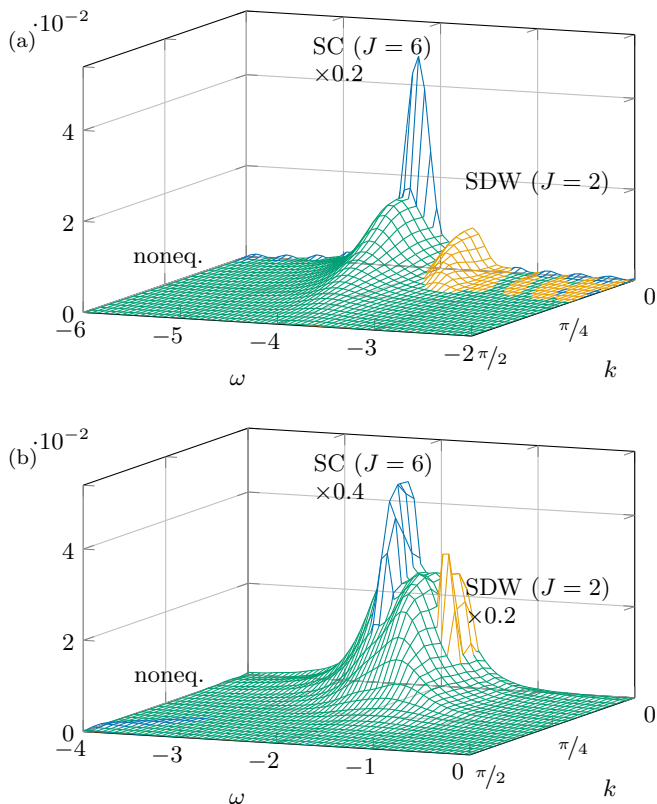


FIG. 4. Comparison of the peak positions of (a) the singlet pair spectral function (cf. Fig. 2) and (b) the single-particle spectral function (cf. Fig. 3) for the spin-density wave and superconducting equilibrium states as well as the nonequilibrium state, respectively. In (a) the spectral peak position is a hybrid of the SDW and SC peaks, whereas in (b) the spectral weight has clearly shifted towards the SC peak.

COMPARISON TO FINITE-TEMPERATURE STATES

All our simulations were performed on pure states that are either ground-states of the models under consideration or quenches from the latter. The question arises whether, following the quench, the system reaches a state in which local observables are thermalized towards their values in the canonical ensemble. To address this issue, we calculated the density matrix $\hat{\rho}(\beta)$ in the SC phase where we choose the inverse temperature $\beta \equiv 1/T$ in a way that $\langle \hat{H} \rangle_\beta \equiv \langle H \rangle_0$. Here, $\langle \dots \rangle_0$ denotes the expectation value of \hat{H} after the quench and $\langle \dots \rangle_\beta$ is the expectation value of \hat{H} with respect to a thermal state $\hat{\rho}(\beta)$ in the superconducting phase. In order to obtain the correct inverse temperature, we performed an imaginary time evolution on an infinite-temperature state $\hat{\rho}(0)$ and cooled down the system this way until the energy matched the one of the quenched state [3]. In Fig. 6, the obtained relation between energy and inverse temperature is displayed with the energy of the quenched state

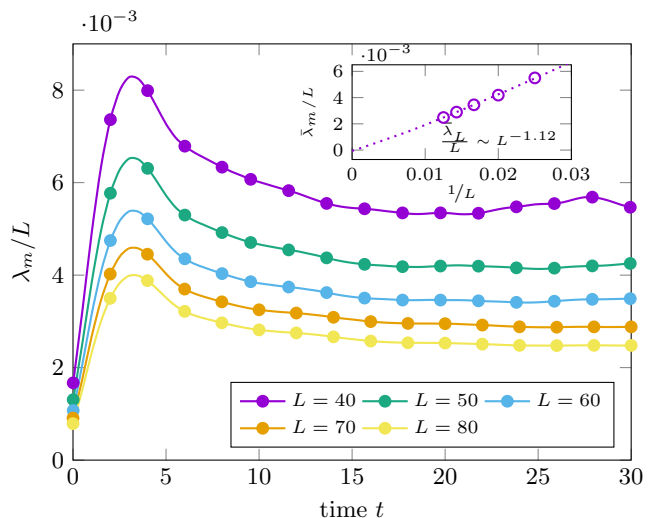


FIG. 5. Time evolution of the largest natural orbital for the quench in the t - J_\perp model; the transient state is reached after about 20 time units. Inset: extrapolated scaling of the normalized dominating eigenvalue $\bar{\lambda}_L/L$ of the correlation matrix with the system size L .

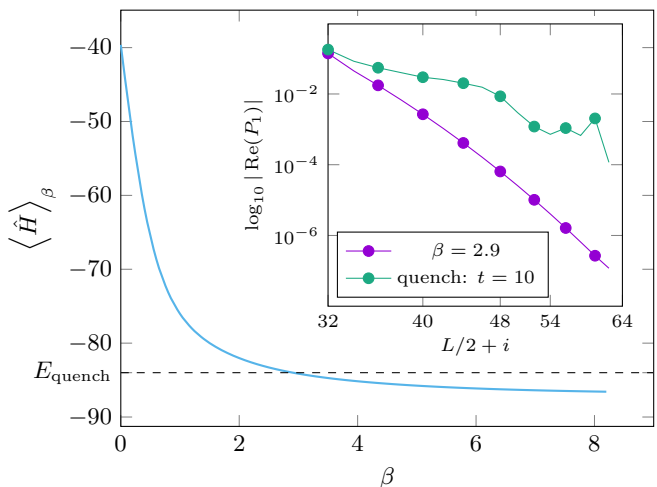


FIG. 6. Energy $\langle \hat{H} \rangle_\beta$ during imaginary time evolution of a system with $L = 32$ sites over imaginary time β . The inset shows the superconducting correlation function $P_1(L/2)$ during the time evolution after a global quench from the CDW to the SC phase at time step $t = 10$ (green), and in a thermal state with $\langle \hat{H} \rangle_\beta$ corresponding to the energy of the quenched system E_{quench} (purple).

marked as dashed line. Having found the respective density matrix $\hat{\rho}(\beta_Q)$, we plot the expectation value of the superconducting correlation function

$$\hat{P}_1(i, j) = \hat{c}_{i,\uparrow}^\dagger \hat{c}_{i,\downarrow}^\dagger \hat{c}_{j,\uparrow} \hat{c}_{j,\downarrow} \quad (25)$$

in both the thermal state and the quenched state at $t = 10$ in the inset of Fig. 6. As can be seen, we do not obtain a state that is characterized by a thermal density matrix

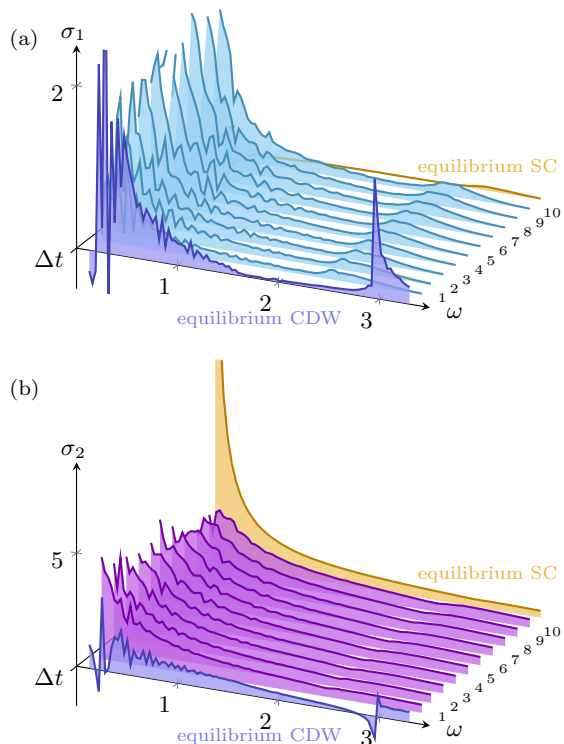


FIG. 7. Real (a) and imaginary (b) part of the optical conductivity $\sigma_{1,2}(\omega, \Delta t)$ with probe pulses applied at different time delays Δt for the quench within the CDW phase ($U = -4t \rightarrow U = -2t$) and the corresponding quantities in the CDW ground state (violet) and the SC ground state (orange).

with inverse temperature β_Q chosen in a way such that its energy matches the one after the quench.

QUENCH WITHIN THE CDW PHASE

In this section we aim to demonstrate that enhanced superconductivity and an enhanced mobility of charge carriers are hard to distinguish if the only information at hand is the optical conductivity. For this purpose we discuss a complementary quench from the charge-density wave (CDW) phase ($U = -4$, $V = 1/4$) – as in the main text – to a point in the CDW phase ($U = -2$, $V = 1/4$) which exhibits a higher metalliticity. Similar analysis of the optical conductivity and the spectral functions of the one- and two-particle excitations as in the main text are done. Furthermore, we show the energy scales after this quench compared to the quench in the main text.

Optical Conductivity

In Fig. 7 the optical conductivity after the quench within the CDW phase is shown. The data is more noisy compared to the case of a quench into the SC phase

which is related to the observation that here the response current exhibits oscillations with larger amplitude and slower decay compared to a quench into the SC phase. We address this to the fact that in the insulating CDW phase there are various scattering processes between the particles. In order to properly resolve the frequency dependencies of these processes the simulation time-range after applying the probe pulse needed to be increased way beyond what was computationally feasible.

Figure 7a displays the real part of the optical conductivity where we find a weak transfer of spectral weight towards smaller frequencies. The imaginary part Fig. 7b also shows an increased spectral weight towards smaller frequencies compared to the equilibrium case. Therefore, without having a reference curve of the system being in the superconducting phase the only possible observation would be a redistribution of spectral weight towards smaller frequencies which may also be interpreted as a sign for enhanced superconductivity. In particular σ_2 suggests that a $1/\omega$ behavior can be realized after the quench if we also take into consideration that due to the finite simulation time $t = 25/t_{\text{hop}}$ after applying the probe pulse the minimally achieved frequency resolution is bounded by $2\pi/25t_{\text{hop}}$.

Spectral Functions

In contrast to the optical conductivity, in the spectral functions we find clearly distinguishable features belonging either to the elementary excitations of the SC or CDW phase. In Figs. 8 and 9 the spectral functions of two- and single-particle excitations are shown, respectively. For easier comparison, the ground states of the SC and the CDW phase, and the quench into the SC phase are included in both figures. The two-particle spectral function Fig. 8 shows a continuum of excitations at small frequencies which is to be contrasted with the sharp excitations in the SC phase. Interestingly, we also find a weak transfer of spectral weight towards $k = 0$ after the quench which we relate to the enhanced metalliticity in the post-quench state. However, the formation of a condensate is suppressed by the continuum at smaller frequencies. On the other hand, in the single-particle spectral function Fig. 9 the identification of the excitation spectrum with either the SC or the CDW phase is not possible, unambiguously. Both findings are consistent with the results discussed above and in the main text supporting our picture that the two-particle spectral function is a more reliable indicator for enhanced superconductivity.

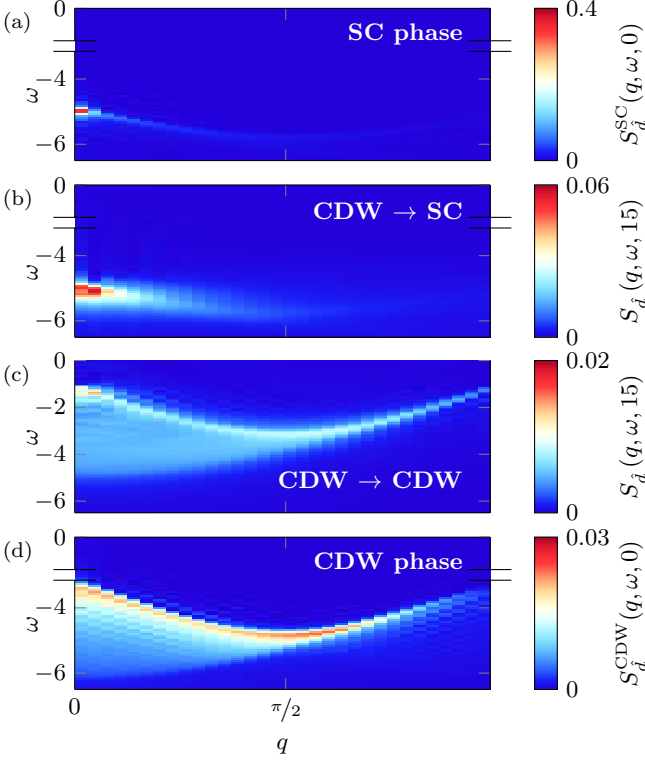


FIG. 8. Comparison between spectral functions of two-particle excitations (a) in the SC ground state, (b) after a quench from the CDW phase to the SC phase, (c) after a quench from the CDW phase to a more metallic point in the CDW phase ($U = -2$, $V = 1/4$). Note that we do not show the full frequency scale, because there is no significant spectral weight in the region we left out.

COHERENT AND DISSIPATIVE CHARGE FLOW

In this section we consider the charge transport in a one-dimensional extended Hubbard model in its SC and CDW ground states, respectively, after excitation with a probe pulse. For this purpose we calculated the time-dependent charge densities after applying a probe pulse

$$A(t, \Delta t) = A_0 e^{-\frac{(t-\Delta t)^2}{2\tau^2}} \cos(\omega_0 t), \quad (26)$$

with $A_0 = 0.5$, $\Delta t = 0.0$, $\tau = 0.05$ and $\omega_0 = 2.38$ in both ground states. Figure 10 displays the induced charge flow

$$\Delta n_i(t) = \langle \hat{n}_i(t) \rangle_{\text{probe}} - \langle \hat{n}_i \rangle_0 \quad (27)$$

where we subtracted the equilibrium value $\langle \hat{n}_i \rangle_0$. Being in the linear response regime this quantity constitutes a measure for the charge transport caused by an optical excitation. Since the system we are considering is calculated using open boundary conditions, the question arises how coherent charge transport in the superconducting phase manifests itself. In Fig. 10a (see also the inset of Fig. 1c in the main text) this is demonstrated in the superconducting phase ($U/t_{\text{hop}} = -4$, $V/t_{\text{hop}} = -1/4$). The

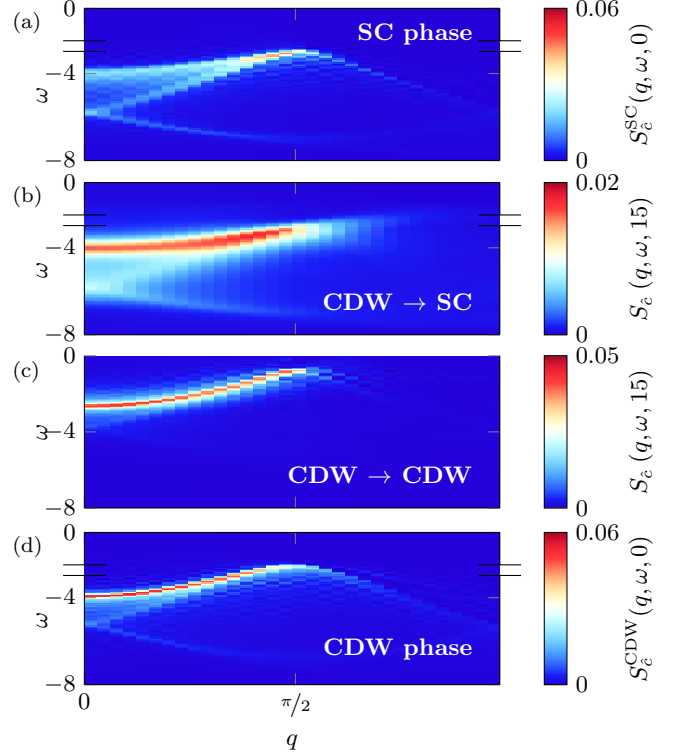


FIG. 9. Spectral functions of single-particle excitations analog to Fig. 8. Note that we do not show the full frequency scale, because there is no significant spectral weight in the region we left out.

probe pulse creates charge accumulation at the boundaries of the system, which act as topological defects. Importantly, the resulting charge flow is nearly dissipationless and we find perfect reflection at the boundaries indicating a long-lived induced current. We interpret our findings as a one-dimensional analogy of the Meissner effect. In contrast in Fig. 10b the induced charge flow in the charge density wave phase ($U/t_{\text{hop}} = -4$, $V/t_{\text{hop}} = 1/4$) is shown after exciting the system. Again, the effect of the probe pulse is to accumulate charge at the boundaries. However, here we find strong scattering processes rendering the charge flow dissipative.

CHECK FOR CONVERGENCE

In order to check the results for convergence we performed simulations with reduced maximal bond dimension $m_{\text{max}} = 500$. In Figs. 11 and 12, the calculated spectral functions of two- and single-particle excitations for those bond dimensions are shown. The fidelity is very high, only small derivations around $q = 0$ are visible, which we relate to an induced length scale due to the truncation errors, but are not relevant for the scope of our investigations. Those derivations are shown in more detail in Figs. 13 and 14 for modes near $q = 0$. As ex-

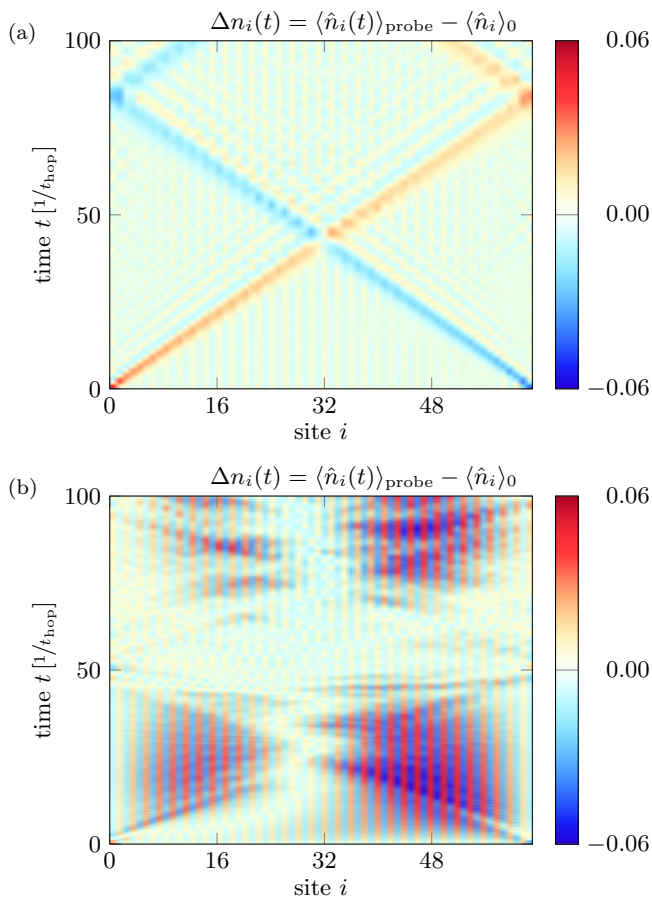


FIG. 10. Induced charge flow $\Delta n_i(t) = \langle \hat{n}_i(t) \rangle_{\text{probe}} - \langle \hat{n}_i \rangle_0$ after applying a probe pulse $A(t, \Delta t) = A_0 e^{-\frac{(t-\Delta t)^2}{2\tau^2}} \cos(\omega_0 t)$ with $\Delta = 0.0$, $\tau = 0.05$ and $\omega_0 = 2.38$ in (a) the superconducting and (b) the charge density wave phase. Coherent transport is seen in the superconducting phase where charge is accumulated at the boundaries and flows coherently after the probe pulse has passed the system. In the charge density wave phase scattering processes destroy the coherence yielding dissipative transport.

pected the spectral functions obtained with higher maximal bond dimension resolve more features. The probably most interesting one can be found in the two-particle spectral functions Fig. 14. Therein, an additional peak structure appears suggesting further fine features, which will be interesting to study in future work.

[1] S. R. White, Phys. Rev. Lett. **69**, 2863 (1992).
 [2] U. Schollwöck, Annals of Physics **326**, 96 (2011).
 [3] S. Paeckel, T. Köhler, A. Swoboda, S. R. Manmana, U. Schollwöck, and C. Hubig, Annals of Physics **411**, 167998 (2019).
 [4] M. B. Hastings, Journal of Statistical Mechanics: Theory and Experiment **2007**, P08024 (2007).

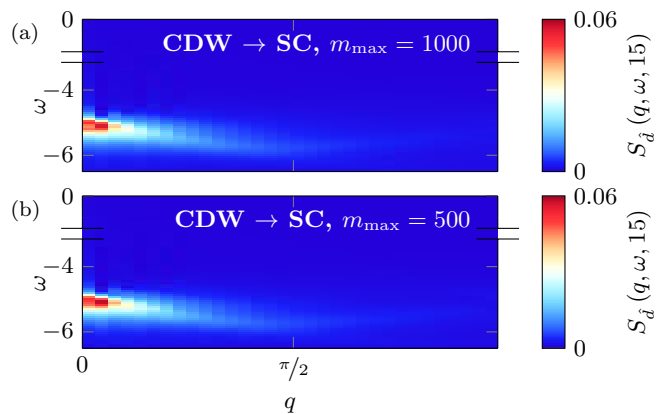


FIG. 11. Spectral functions of two-particle excitations after quenching $V = 0.25 \rightarrow V = -0.25$ with (a) $m_{\text{max}} = 1000$ and (b) $m_{\text{max}} = 500$. Note that we do not show the full frequency scale, because there is no significant spectral weight in the region we left out.

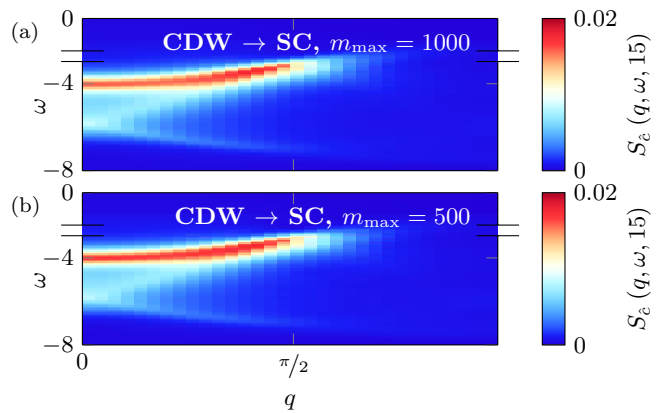


FIG. 12. Spectral functions of single-particle excitations after quenching $V = 0.25 \rightarrow V = -0.25$ with (a) $m_{\text{max}} = 1000$ and (b) $m_{\text{max}} = 500$. Note that we do not show the full frequency scale, because there is no significant spectral weight in the region we left out.

[5] F. Verstraete and J. I. Cirac, Phys. Rev. B **73**, 094423 (2006).
 [6] J. Haegeman, C. Lubich, I. Oseledets, B. Vandereycken, and F. Verstraete, Phys. Rev. B **94**, 165116 (2016).
 [7] S. Paeckel and T. Köhler, The SYMMPS Toolkit, <https://www.symmps.eu>, accessed: 2019-12-29.
 [8] O. Penrose and L. Onsager, Phys. Rev. **104**, 576 (1956).
 [9] I. Rousochatzakis, S. R. Manmana, A. M. Läuchli, B. Normand, and F. Mila, Phys. Rev. B **79**, 214415 (2009).
 [10] N. D. Mermin and H. Wagner, Phys. Rev. Lett. **17**, 1133 (1966).
 [11] N. D. Mermin and H. Wagner, Phys. Rev. Lett. **17**, 1307 (1966).
 [12] P. C. Hohenberg, Phys. Rev. **158**, 383 (1967).
 [13] M. Rigol and A. Muramatsu, Phys. Rev. A **70**, 031603 (2004).
 [14] M. Rigol and A. Muramatsu, Phys. Rev. A **72**, 013604 (2005).

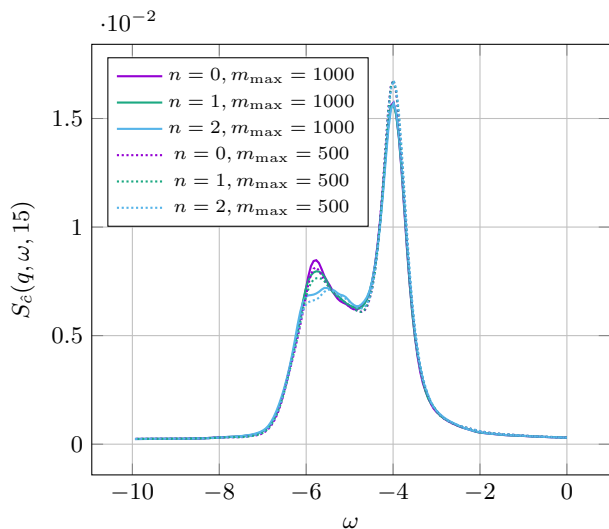


FIG. 13. Comparison of single-particle spectral functions $S_e(q, \omega, 15)$ after quenching $V = 0.25 \rightarrow V = -0.25$ evaluated at fixed values of the wave vector $q_n = \frac{2\pi}{L-1}n$ and for maximal bond dimensions $m_{\max} = 500, 1000$.

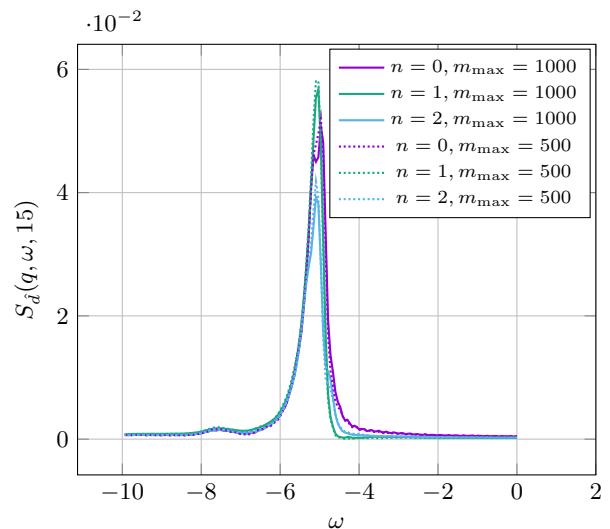


FIG. 14. Comparison of two-particle spectral functions $S_d(q, \omega, 15)$ after quenching $V = 0.25 \rightarrow V = -0.25$ evaluated at fixed values of the wave vector $q_n = \frac{2\pi}{L-1}n$ and for maximal bond dimensions $m_{\max} = 500, 1000$.

- [15] A. V. Gorshkov, S. R. Manmana, G. Chen, J. Ye, E. Demler, M. D. Lukin, and A. M. Rey, *Phys. Rev. Lett.* **107**, 115301 (2011).
- [16] S. R. Manmana, M. Möller, R. Gezzi, and K. R. A. Hazzard, *Phys. Rev. A* **96**, 043618 (2017).
- [17] T. Giamarchi, *Quantum Physics in One Dimension*, Vol. 121 of *International Series of Monographs on Physics* (Oxford University Press, Oxford, 2004).